

Diagnosis of transport properties in Ferromagnets

Andrew Das Arulsamy¹

¹*Condensed Matter Group, Division of Exotic Matter, No. 22,
Jalan Melur 14, Taman Melur, 68000 Ampang, Selangor DE, Malaysia*

(Dated: May 1, 2019)

The ionization energy based resistivity model with further confinements from spin-disorder scattering and polaronic effect is derived so as to capture the mechanism of both spin independent and spin-assisted charge transport in ferromagnets. The computed $T_{crossover}$ below T_C and carrier density in $Ga_{1-x}Mn_xAs$ ($x = 6-7\%$) are 8-12 K and 10^{19} cm^{-3} , identical with the experimental values of 10-12 K and $10^{18}-10^{20} \text{ cm}^{-3}$ respectively. The calculated charge densities for $Mn_{0.02}Ge_{0.98}$ and $La_{1-x}Ca_xMnO_3$ ($x = 10-20\%$) are 10^{19} cm^{-3} and 10^{17} cm^{-3} respectively.

PACS numbers: 75.70.-i; 71.30.+h; 72.15.Rn; 75.50.Pp

Keywords: Ferromagnets, Fermi-Dirac statistics, Ionization energy, Resistivity model

1. Introduction

Diluted magnetic semiconductors (DMS) have the tremendous potential for the development of spintronics and subsequently will lay the foundation to realize quantum computing. In order to exploit the spin assisted charge transport, one needs to understand the transport mechanism such as the variation of resistivity with temperature and doping in both paramagnetic and ferromagnetic phases. A wide variety of the magneto-electronic properties based on doping and Mn's valence state in manganites were reported to understand the transport mechanism(s) [1, 2]. Among them, the influence of grain boundary as a barrier [3], as a region of depleted T_C [4] and polaronic effect [5] on electrical properties were reported. Direct proportionality of \mathbf{H} with T_C [6] and resistivity with defects or substrate-film lattice incompatibility [7, 8, 9, 10, 11] are also regarded as equally important to determine the electrical properties of manganites. Furthermore, metallic conduction below T_C has been studied using double exchange mechanism (DEM) between s and d orbitals [12] and the displacement of hysteresis loop in field-cooled sample with an additional scenario of non-linear spin and charge fluctuations due to magnon [13]. Explanations in term of hopping electrons and DEM [14], and the influence of microstructural transition arises from ionic radius or valence state of Nd in $Nd_xSm_{1-x}Ca_{0.8}MnO_3$ [15] were also reported extensively. The effect of hydrostatic (external) pressure ($P = 0 \rightarrow 15$ kbar) and chemical doping (internal P) on metal-insulator transition of Pr-Ca,La-Sr-MnO₃ have been reported as well. [16].

Interestingly, Van Esch *et al.* [17] have proposed multiple exchange interactions, which are ferromagnetic (FM) hole-hole and antiferromagnetic (AFM) Mn-hole interactions for DMS. These two effects, after neglecting the direct exchange between Mn-Mn (due to very diluted nature of DMS) are seem to be sufficient enough to describe the temperature dependent magnetization curves ($M(T)$) accurately. However, even after inclusion of FM

and AFM effects including the spin disorder scattering, the transport property in the FM phase is still not well understood. Unfortunately, this is also true for the case of metallic property below T_C in the well known and extensively studied FM manganites as pointed out by Mahendiran *et al.* [18]. The resistivity ($\rho(T)$) above T_C for manganites is found to be in an activated form described by the equation [18],

$$\rho(T > T_C) = \rho_0 \exp\left(\frac{E_a}{k_B T}\right). \quad (1)$$

E_a is the activation energy, ρ_0 and k_B denote the residual resistivity at $T \gg E_a$ and Boltzmann constant respectively. In the FM phase, the influence of $M(T)/M_0$ is more pronounced than the electron-phonon ($e-ph$) contribution where the latter requires an overwhelmingly large coupling constant [18]. Note that M_0 is the magnitude of magnetization at 0 K. Therefore, Mahendiran *et al.* have suggested that conventional mechanism namely, $e-ph$ scattering has to be put aside so as to explain the $\rho(T)$ for manganites below T_C . On the contrary, $\rho(T)$ with $e-ph$ involvement for DMS in the paramagnetic phase is given by [17]

$$\rho(T > T_C) = \frac{C_1 + C_2 [\exp(\Theta_D/T) - 1]^{-1}}{k_B T \ln [1 + \exp((E_m - E_f)/k_B T)]}. \quad (2)$$

The term, $C_2/[\exp(\Theta_D/T) - 1]$ takes care of the $e-ph$ contribution. Θ_D , E_f , E_m , C_1 and C_2 represent the Debye temperature, Fermi level, mobility edge and numerical constants respectively. The $\rho(T)$ in the FM phase based on the spin disorder scattering as derived by Tinbergen-Dekker is given by [19]

$$\begin{aligned} \rho_{SD}(T < T_C) &= \frac{(m_{e,h}^*)^{5/2} N (2E_F)^{1/2}}{\pi(n,p)e^2 \hbar^4} J_{ex}^2 \\ &\times \left[S(S+1) - S^2 \left(\frac{M_{TD}(T)}{M_0} \right)^2 - S \left(\frac{M_{TD}(T)}{M_0} \right) \right] \end{aligned}$$

$$\times \tanh \left(\frac{3T_C M_{TD}(T)}{2TS(S+1)M_0} \right). \quad (3)$$

N is the concentration of nearest neighbor ions (Mn's concentration) while (n, p) is the concentration of charge carriers (electrons or holes respectively). $m_{e,h}^*$ denotes effective mass of electrons or holes, $\hbar = h/2\pi$, $h =$ Planck constant. e is the charge of an electron, E_F and J_{ex} are the Fermi and FM exchange interaction energies respectively while S is the spin quantum number. Equation (3) becomes equivalent to Kasuya [20] if one replaces the term, $\tanh [3T_C M_{TD}(T)/2TS(S+1)M_0]$ with 1. Again, an accurate equation for the $\rho(T)$ below T_C is still lacking since spin disorder scattering alone is insufficient as shown by Tinbergen and Dekker [19] as well as reviewed by Ohno [21].

As a consequence, it is desirable to derive a formula that could describe the transport mechanism of ferromagnets for the whole temperature range i.e., for both paramagnetic and FM phases and even at very low T . With this in mind, the E_I based Fermi-Dirac statistics (iFDS) and spin disorder scattering based resistivity models will be employed in order to derive ρ as a function of T , E_I and $M_\rho(T, M_0)$. The consequences of $\rho(T, E_I, M_\rho(T, M_0))$ that arises from the variation of T , E_I and $M_\rho(T, M_0)$ are discussed in detail based on the experimental data reported by Van Esch *et al.* [17], Mahendiran *et al.* [18] and Park *et al.* [22]. The $\text{Mn}_x\text{Ge}_{1-x}$ FM semiconductor (FMS) is also accentuated here due to its promising properties for device applications [22] where its gate voltage of ± 0.5 V is compatible with the present Complementary Metal-Oxide-Semiconductor (CMOS) and Ge's hole mobility ($110.68 \text{ m}^2\text{V}^{-1}\text{s}^{-1}$) is higher than GaAs ($12.65 \text{ m}^2\text{V}^{-1}\text{s}^{-1}$) and Si ($15.81 \text{ m}^2\text{V}^{-1}\text{s}^{-1}$). $\text{Mn}_x\text{Ge}_{1-x}$'s resistivity is also semiconductor-like below T_C , which is more suitable than metallic $\text{Ga}_{1-x}\text{Mn}_x\text{As}$. Moreover, $\text{Mn}_x\text{Ge}_{1-x}$ is also the simplest two-element system that can be utilized to evaluate the performance of the derived model consists of iFDS and $M_\alpha(T)$ (originates from τ_{SD}). $\alpha = \text{K}$ (calculated from the Kasuya's spin disorder scattering model), ρ (calculated from the resistivity model), exp (determined experimentally).

2. Resistivity model

The total current in semiconducting ferromagnets with contributions from both paramagnetic and FM phases is $J = \sum_\nu J_\nu$, $\nu = e^\downarrow, se^\uparrow, h^\downarrow, sh^\uparrow$. For convenience, the spin-up, \uparrow denotes the direction of the magnetic field or a particular direction below T_C , while the spin-down, \downarrow represents any other directions. Note that the total energy (Kinetic + Magnetic), $E_{K+M}^\uparrow \neq E_{K+M}^\downarrow$ due to energy level splitting below T_C . As such, the total current can be simplified as $J = J_e^\downarrow + J_{se}^\uparrow = J_e + J_{se}$ if the considered system is an n -type while $J = J_h + J_{sh}$ if it is a p -type.

J_e and J_h are the spin independent charge current (electrons and holes respectively) in the paramagnetic phase whereas J_{se} and J_{sh} are the spin-assisted charge current in the FM phase. Thus the total resistivity (n or p -type) can be written as

$$\begin{aligned} \rho^{-1} &= \rho_{e,h}^{-1} + \rho_{se,sh}^{-1} \\ &= \left[\frac{m_{e,h}^*}{(n,p)e^2\tau_e} \right]^{-1} + \left[\frac{m_{e,h}^*}{(n,p)e^2\tau_{SD}} \right]^{-1}. \end{aligned} \quad (4)$$

τ_{SD} represents the spin disorder scattering rate. The carrier density for the electrons and holes (n, p) based on iFDS are given by [23, 24, 25, 26, 29]

$$n = 2 \left[\frac{k_B T}{2\pi\hbar^2} \right]^{3/2} (m_e^*)^{3/2} \exp \left[\frac{E_F - E_I}{k_B T} \right]. \quad (5)$$

$$p = 2 \left[\frac{k_B T}{2\pi\hbar^2} \right]^{3/2} (m_h^*)^{3/2} \exp \left[\frac{-E_F - E_I}{k_B T} \right]. \quad (6)$$

iFDS is derived in a latter section in which, its applications are well documented in the Refs. [23, 24, 25, 26, 27, 28, 29, 30]. Substituting $1/\tau_e = AT^2$ (due to electron-electron interaction), Eqs. (3) and (5) or (6) into Eq. (4), then one can arrive at

$$\rho_{e,se}(T) = \frac{AB \exp [(E_I + E_F)/k_B T]}{AT^{3/2} [M_\rho(T, M_0)]^{-1} + BT^{-1/2}}. \quad (7)$$

In which, $A = [A_{e,h}/2e^2(m_{e,h}^*)^{1/2}][2\pi\hbar^2/k_B]^{3/2}$, $B = 2m_{e,h}^*N(\pi E_F)^{1/2}J_{ex}^2/e^2\hbar k_B^{3/2}$ and $\tau_{SD}^{-1} = [N(2E_F)^{1/2}(m_{e,h}^*)^{3/2}/\pi\hbar^4]J_{ex}^2M_\rho(T, M_0)$. $A_{e,h}$ is the T independent electron-electron scattering rate constant. The E_I here takes care of the polaronic effect or more precisely, the electron-phonon interaction. The empirical function of the normalized magnetization is given by

$$M_\rho(T, M_0) = 1 - \frac{M_\rho(T)}{M_0}. \quad (8)$$

Equation (8) is an empirical function that directly quantifies the influence of spin alignments in the FM phase on the transport properties of charge and spin carriers in accordance with Eq. (7). In other words, the only way to obtain $\frac{M_\rho(T)}{M_0}$ is through Eq. (8). In fact, Eq. (8) is used to calculate $M_{TD}(T)/M_0$ and $M_K(T)/M_0$ by writing $S(S+1) - S^2(\frac{M_{TD}(T)}{M_0})^2 - S(\frac{M_{TD}(T)}{M_0}) \tanh [\frac{3T_C M_{TD}(T)}{2TS(S+1)M_0}] = M_\rho(T, M_0)$ and $S(S+1) - S^2(\frac{M_K(T)}{M_0})^2 - S(\frac{M_K(T)}{M_0}) = M_\rho(T, M_0)$ respectively. Consequently, one can actually compare and analyze the

$M_\alpha(T)/M_0$ ($\alpha = \text{TD, K, } \rho$) calculated from Tinbergen-Dekker (TD), Kasuya (K) and Eq. (7) with the experimentally measured $M_{exp}(T)/M_0$. However, one has to switch to Eq. (9) given below for the hole-doped strongly correlated paramagnetic semiconductors, which is again based on iFDS [23, 27],

$$\rho_h = \frac{A_h(m_h^*)^{-1}}{2e^2} \left[\frac{2\pi\hbar^2}{k_B} \right]^{3/2} T^{1/2} \exp \left[\frac{E_I + E_F}{k_B T} \right]. \quad (9)$$

A_h is the T independent electron-electron scattering rate constant. Equation (9) will be used to justify the importance of the term J_{se} even if the resistivity is semiconductor-like in the FM phase. Note that, $m^* = m_e^* \approx m_h^* \approx (m_e^* m_h^*)^{1/2}$ is used for convenience. If however, $m_e^* \neq m_h^*$, then one just has to use the relation, $m^* = m_e^* m_h^* / (m_e^* + m_h^*)$. Even in the usual consideration for the total conductivity, $\sigma = \sigma_{electron} + \sigma_{hole}$, some algebraic rearrangements can lead one to the relation, $\rho(T) \propto \exp(E_I/k_B T) / [\exp(E_F/k_B T) + \exp(-E_F/k_B T)]$, exposing the consistent effect of E_I on transport properties.

3. Discussion

3.1. Temperature-dependent resistivity curves

Resistivity versus temperature measurement ($\rho(T)$) is the most simplest and effective method to study the transport properties. In free-electron metals, the $\rho(T)$ curves are often exploited in order to deduce the T -dependence of the scattering rates namely, τ_{e-e} and τ_{e-ph} . Such behavior are well described by the Bloch-Grüneisen (BG) formula [31], given by

$$\rho_{BG} = \lambda_{tr} \frac{128\pi m^* k_B T^5}{n e^2 \Theta_D^4} \int_0^{\Theta_D/2T} \frac{x^5}{\sinh^2 x} dx. \quad (10)$$

λ_{tr} = electron-phonon coupling constant, n = free electrons concentration. The approximation of $\tau_{e-e}(T)$ and $\tau_{e-ph}(T)$ using Eq. (10) is valid basically because there are no other parameters that vary with T , apart from the said scattering rates. In fact, by utilizing the BG formula, one can reliably estimate that $\tau_{e-e}(T) \propto T^{-2}$ while $\tau_{e-ph}(T) \propto T^{-3 \rightarrow -5}$ for any experimentally viable Θ_D .

On the other hand, the metallic phenomenon observed in the ferromagnetic-metallic (FMM) phase below T_C in ferromagnets (FM) cannot be characterized as Fermi gas. Therefore, it is rather incorrect to extract $\tau_{e-e}(T)$, $\tau_{e-ph}(T)$ and $\tau_{magnons}(T)$ from the $\rho(T < T_C)$ curves in FM. Experimental evidences based on the photoemission, X-ray emission/absorption and extended X-ray

emission fine structure spectroscopy have exposed the polaronic effect even at $T < T_C$ or in the FMM phase [32]. Consequently, the charge density (n) in FMM phase is not T independent as one would anticipate for the free-electron metals (Fermi-gas). In addition, spin related mechanisms, like magnons and spin disorder scattering can be correctly represented with the normalized magnetization function, $M(T, M_0)$. It is quite common to employ Matthiessen's rule ($\tau^{-1} = \sum_i \tau_i^{-1}$) as opposed to the total current rule ($\tau = \sum_i \tau_i$) and write the resistivity below T_C in the form of

$$\rho(T) = \rho_0 + \sum_i A_i T^{\alpha_i}. \quad (11)$$

The i here indicates the types of T -dependent scattering rate that contribute to the resistivity and A is a T independent constant. ρ_0 is the T -independent scattering rate that originates from the impurities as $T \rightarrow 0$ K. The critical issue here is not about the Matthiessen's rule, but on the validity of Eq. (11) in non free-electronic phase. Importantly, the T -dependent structure of Eq. (10) is equivalent to Eq. (11) that actually have enabled one to reliably calculate $\tau_{e-e}^{-1}(T)$ and $\tau_{e-ph}^{-1}(T)$ as $A_{e-e} T^2$ and $A_{e-ph} T^{3 \rightarrow 5}$ respectively. Equation (11) is extremely popular and it is applied indiscriminately to determine the T -dependence of a wide variety of scattering rates in FMM phase, while the correctness of such determination is still unclear and varies from one researcher to another [18, 33, 34]. It is important to realize that only a free-electronic FMM phase at $T < T_C$ will justify the analysis based on Eq. (11). The influence of polaronic effect and magnetization function (the variation of $M(T)/M_0$ with T) reinforces the T -dependence of charge density, which point towards the inapplicability of Eq. (11) in FMM phase.

3.2. $\text{Ga}_{1-x}\text{Mn}_x\text{As}$

The resistivity measurements [17] and its fittings based on Eqs. (7) and (9) are shown in Fig. 1 a) and b) respectively for $\text{Ga}_{1-x}\text{Mn}_x\text{As}$. One needs two fitting parameters (A and E_I) for $\rho(T > T_C)$ and another two (B and $M_\rho(T, M_0)$) for $\rho(T < T_C)$. All the fitting parameters are listed in Table I. Note that $S = 1$ and $5/2$ are employed for the fittings of $M_K(T)/M_0$ while T_C and $T_{crossover} = T_{cr}$ were determined from the experimental resistivity curves. The deviation of $M_K(T)/M_0$ from the M_{exp}/M_0 increases with S from $1 \rightarrow 5/2$. The $\rho(T)$ is found to increase with x from 0.060 to 0.070 due to the mechanism proposed by Van Esch *et al.* [17, 35] and Ando *et al.* [36]. They proposed that neutral Mn^{3+} acceptors that contribute to magnetic properties could be compensated by As, where for a higher concentration of

Mn, instead of replacing Ga it will form a six-fold coordinated centers with As ($\text{Mn}^{6\text{As}}$) [17, 35, 36]. These centers will eventually reduce the magnitude of ferromagnetism (FM) in DMS due to the loss of spin-spin interaction between $\text{Mn}(3d^5)$ and h . iFDS based resistivity models also predicts that if one assumes Mn^{2+} ($E_I = 1113 \text{ kJmol}^{-1}$) or Mn^{3+} ($E_I = 1825 \text{ kJmol}^{-1}$) substitutes Ga^{3+} ($E_I = 1840 \text{ kJmol}^{-1}$), then $\rho(T)$ should further decrease with x , which is not the case here. Thus, iFDS also suggests that Mn^{2+} or Mn^{3+} do not substitute Ga^{3+} . Interestingly, the T_{cr} s observed in $\text{Ga}_{0.940}\text{Mn}_{0.060}\text{As}$ (annealed: 370°C) and $\text{Ga}_{0.930}\text{Mn}_{0.070}\text{As}$ (as grown) are 10 K and 12 K, which are identical with the calculated values of 8 K and 12 K respectively. Note here that $E_I + E_F = T_{cr}$. The calculated carrier density using $E_I + E_F$ (8, 12 K), m_h^* = rest mass and Eq. (6) is $2.4 \times 10^{19} \text{ cm}^{-3}$. Below T_C , spin alignments enhance the contribution from J_{se} and reduces the exponential increase of $\rho(T)$. This reduction in $\rho(T)$ is as a result of dominating J_{se} and the small magnitude of $E_I + E_F$ (8 K, 12 K), consequently its effect only comes at low T as clearly shown in Fig. 1 a). The $\text{Ga}_{0.930}\text{Mn}_{0.070}\text{As}$ samples after annealing at 370°C and 390°C do not indicate any FM [17] (Fig. 1 b)). Thus the fittings are carried out with Eq. (9) that only requires two fitting parameters namely, A and $E_I + E_F$ since $J_{se} = 0$ (there is no observable T_C) and/or $dM_\alpha(T)/M_0dT = 0$ ($M_\rho(T, M_0) = \text{constant}$). The exponential increase in Fig. 1 b) for $\rho(T)$ is due to $E_I + E_F$ from Eq. (9) with zilch J_{se} contribution.

Figure 1 c) and d) indicate the normalized magnetization, $M_\alpha(T)/M_0$. Note that $M_{\rho,TD,K}(T)/M_0$ is a fitting parameter that has been varied accordingly to fit $\rho(T < T_C)$. $M_\rho(T, M_0)$ is used to calculate $M_{\rho,TD,K}(T)/M_0$ with $S = 1$. $M_{\rho,TD,K}(T)/M_0$ is also compared with the experimentally determined [17] $M_{exp}(T)/M_0$ as depicted in Fig. 1 d). One can easily notice the inequality, $M_{TD}(T)/M_0 > M_K(T)/M_0 > M_\rho(T)/M_0 > M_{exp}(T)/M_0$ from Fig. 1 c) and d). As such, $M_\rho(T)/M_0$ from Eq. (7) is the best fit for the experimentally measured $M_{exp}(T)/M_0$. However, $M_\rho(T)/M_0$ is still larger than $M_{exp}(T)/M_0$, because resistivity measures only the path with relatively lowest E_I and with easily aligned spins that complies with the principle of least action. On the contrary, the magnetization measurement quantifies the average of all the spins' alignments.

3.3. $\text{La}_{1-x}\text{Ca}_x\text{MnO}_3$

Mahendiran *et al.* [18] discussed $\rho(T < T_C)$ with respect to Eq. (1) and obtained the activation energy, $E_a = 0.16 \text{ eV}$ for $x = 0.1$ and 0.2 of $\text{La}_{1-x}\text{Ca}_x\text{MnO}_3$ samples at 0 T. Using Eq. (7) however, $E_I + E_F$ for the former and latter samples are calculated to be 0.12 and 0.11 eV respectively. The calculated carrier density using $E_I + E_F$ ($0.12, 0.11 \text{ eV}$), m_h^* = rest mass and Eq. (6)

is approximately 10^{17} cm^{-3} . In the presence of $\mathbf{H} = 6 \text{ T}$, $E_I + E_F$ is computed as 0.0776 eV for $x = 0.2$ that subsequently leads to $p = 10^{18} \text{ cm}^{-3}$. It is proposed that the activated behavior for $\rho(T > T_C)$ is due to electron-phonon interaction or rather due to the polaronic effect (E_I) [23]. The fittings are shown in Fig. 2 a) and b) while its fitting parameters are listed in Table I. Theoretically [23], Ca^{2+} ($E_I = 868 \text{ kJmol}^{-1}$) $<$ La^{3+} ($E_I = 1152 \text{ kJmol}^{-1}$), therefore $\rho(T)$ is expected to decrease with Ca^{2+} doping significantly. On the contrary, only a small difference of $E_I + E_F$ between $x = 0.1$ (0.12 eV) and 0.2 (0.11 eV) is observed due to Mn^{4+} 's compensation effect. The quantity, Mn^{4+} increased 6% from $x = 0.1$ (19%) to 0.2 (25%) [18]. Ideally, the difference of E_I between Ca^{2+} and La^{3+} is $1152 - 868 = 284 \text{ kJmol}^{-1}$. As a result of compensation with 6% $\text{Mn}^{3+ \rightarrow 4+}$ ($E_I = 4940 \text{ kJmol}^{-1}$), the actual difference is only $284 - [0.81(1825) + 0.19(4940) - 0.75(1825) - 0.25(4940)] = 97 \text{ kJmol}^{-1}$. This calculation simply exposes the compensation effect.

At 6 T, $\text{La}_{0.8}\text{Ca}_{0.2}\text{MnO}_3$ indicates a much lower resistivity (Fig. 2 b)). The result that larger \mathbf{H} giving rise to overall conductivity is due to relatively large amount of aligned spins that eventually gives rise to J_{se} . Hence, $E_I + E_F$ at 6 T (78 meV) is less than $E_I + E_F$ at 0 T (112 meV). Figure 2 c) and d) depict the calculated $M_\alpha(T)/M_0$ with $S = 1$ and $M_{exp}(T)/M_0$ for $x = 0.2$ respectively. The calculated $M_{TD}(T)/M_0$ is dropped for $\text{La}_{1-x}\text{Ca}_x\text{MnO}_3$ since $M_K(T)/M_0$ seems to be a better approximation than $M_{TD}(T)/M_0$ as indicated in Fig. 1 c) and d). The discrepancy between $M_\rho(T)/M_0$ and $M_{exp}(T)/M_0$ still exists even though Eq. (7) reproduces $\rho(T)$ at all T range accurately. Again, this incompatibility is due to the principle of least action as stated earlier. In addition, the manganites' charge transport mechanism below T_C is also in accordance with Eq. (7) because the term, $M_\rho(T, M_0)$ handles the exchange interactions' complexities separately for DMS and manganites. For example, one can clearly notice the different type of discrepancies between DMS and manganites by comparing the empirical function, $M_\alpha(T)/M_0$ ($\alpha = \rho, \text{exp}$) between Fig. 1 d) and Fig. 2 d). Hence, Eq. (7) is suitable for both types of ferromagnets, be it diluted or concentrated.

3.4. $\text{Mn}_x\text{Ge}_{1-x}$

The $\text{Mn}_x\text{Ge}_{1-x}$ FMS with homogeneous Mn concentration has been grown using low- T MBE technique [22]. The $\text{Mn}_x\text{Ge}_{1-x}$ was found to be a p -type with carrier density in the order of $10^{19} - 10^{20} \text{ cm}^{-3}$ for $0.006 \leq x \leq 0.035$ as measured by Park *et al.* [22]. Both the resistivity measurements [22] and its fittings based on Eq. (7) are shown in Fig. 3 a). Here, $E_I + E_F$, A and B have been floated while $M_\rho(T, M_0)$ is constrained to reduce with T in order to fit the experimental $\rho(T, x = 0.02)$. The absence of

the Curie-Weiss law in the $\rho(T, x = 0.02)$ curve is due to insufficient number of aligned spins that eventually leads to a relatively small J_{se} , which in turn, is not able to produce the metallic conduction below T_C . This scenario is also in accordance with the measured $M_{exp}(T)$ where, only 1.4-1.9 μ_B/Mn atom contributes to ferromagnetism as compared with the ideal value of 3.0 μ_B/Mn atom. In other words, only 45-60% of Mn ions are magnetically active [22]. It is found that $E_I + E_F = 15$ K from the $\rho(T)$ fitting for $\text{Mn}_{0.02}\text{Ge}_{0.98}$. Subsequently, one will be able to calculate the hole concentration as $2.38 \times 10^{19} \text{ cm}^{-3}$ using Eq. (6) and $m_h^* = \text{rest mass}$, which is remarkably in the vicinity of the experimental value [22], $10^{19} - 10^{20} \text{ cm}^{-3}$. Interestingly, the semiconductor-like behavior of $\rho(T, x = 0.02)$ below T_C is *not* exponentially driven as the value of $E_I + E_F$ is very small (15 K) to be able to contribute significantly above 15 K. Rather, it is the T -dependence of Eq. (7) determines $\rho(T, x = 0.02)$ below T_C . To see this clearly, one can actually approximate the experimental $\rho(T, x = 0.02)$ with a mathematical function given by $\rho = -21.711 \times \ln T + 148.47$ (not shown). In this computation, the $\ln T$ behavior is the approximate version for the T -dependence of Eq. (7). Another obvious proof is the inability of Eq. (9) to represent the experimental $\rho(T, x = 0.02)$. The plot using Eq. (9) is also shown in Fig. 3 a) with $A_h = 1.8$ and $E_I + E_F = 80$ K that eventually give $p = 1.92 \times 10^{19} \text{ cm}^{-3}$. However, in the absence of J_{se} term, Eq. (9) is inadequate to capture the T -dependence of $\rho(T, x = 0.02)$ in the FM phase.

The pronounced effect of $M_\rho(T, M_0)$ can be noticed by comparing the calculated plots between Eq. (7) and Eq. (7) with additional constraint, $dM_\rho(T)/dT = 0$ as indicated in Fig. 3 a). Recall that $M_\rho(T, M_0)$ is varied with T to fit the experimental $\rho(T, x = 0.02)$ in compliance with Eq. (7). Furthermore, $\rho(T)$ is found [22] to decrease with x from 0.016 to 0.02 while $\rho(T, x = 0.02)$ remains identical with $\rho(T, x = 0.033)$. This type of transition can be readily evaluated with Eq. (7). Firstly, notice the large increase in room temperature p from 10^{14} cm^{-3} (upper limit) for pure Ge to 10^{19} cm^{-3} (lower limit) for a mere 2% Mn substituted $\text{Mn}_{0.02}\text{Ge}_{0.98}$, which gives rise to a rapid decrease of $\rho(T, x)$. The average E_{I_s} for Mn^{2+} , Mn^{3+} and Ge^{4+} are computed as 1113, 1825 and 2503 kJmol^{-1} respectively. According to iFDS, Mn substitution into Ge sites will reduce the magnitude of $\rho(T)$ since $E_I(\text{Ge}^{4+}) > E_I(\text{Mn}^{3+}) > E_I(\text{Mn}^{2+})$, regardless of $dM(T)/dT = 0$ or $dM(T)/dT \neq 0$. Such behavior has been observed experimentally [22] where, $\rho(T, x = 0.009) > \rho(T, x = 0.016) > \rho(T, x = 0.02)$. This scenario indicates that the holes from $\text{Mn}^{2+,3+}$ is kinetically favorable than the intrinsic holes from Ge^{4+} . It is also found experimentally that $\rho_{rt}(x = 0.009) < \rho_{rt}(x = 0.016)$ as a result of the variation of T independent scattering rate constants (A and B). Surprisingly however, $\rho(T, x = 0.02) \simeq \rho(T, x = 0.033)$, which sug-

gests that A , B and T -dependence of $M_{exp}(T)/M_0$ are identical. Using iFDS, one should get $\rho(T, x = 0.02) > \rho(T, x = 0.033)$ and $[A, B]_{x=0.02} > [A, B]_{x=0.033}$. Meaning, the additional Mn substitution ($0.033 - 0.02 = 0.013$) may not have substituted Ge, instead it could have formed a well segregated impurity phase that eventually contributes to the higher magnitudes of A and B ($[A, B]_{x=0.02} \approx [A, B]_{x=0.033}$), and consequently does not interfere with the $M_{exp}(T)/M_0$. Notice that the formation of impurity phase is quite common in any system, including $\text{Ga}_{1-x}\text{Mn}_x\text{As}$ DMS with strictly limited Mn solubility. On the other hand, the normalized magnetization, $M_{K,\rho,exp}(T)/M_0$ for $\text{Mn}_{0.02}\text{Ge}_{0.98}$ have been plotted in Fig. 3 b). One can notice the relation, $M_K(T)/M_0 > M_\rho(T)/M_0 > M_{exp}(T)/M_0$ from Fig. 3 b). Again, $M_\rho(T)/M_0 > M_{exp}(T)/M_0$ is due to the ability of both J_e and J_{se} to follow the easiest path. Additionally, the T -dependence of $M_{exp}(T)$ is similar to $\text{Ga}_{1-x}\text{Mn}_x\text{As}$ rather than the well established manganite ferromagnets, which reveals the possibility of multiple exchange interactions [17, 22, 35]. All the values of E_I discussed above were averaged in accordance with $E_I[X^{z+}] = \sum_{i=1}^z \frac{E_{I_i}}{z}$. Prior to averaging, the 1st, 2nd, 3rd and 4th ionization energies for all the elements mentioned above were taken from Ref. [37].

4. iFDS

Here, the Lagrange multipliers, degeneracy and the total energy requirement associated with E_I in iFDS is discussed in detail. Both FDS and iFDS are for the half-integral spin particles such as electrons and holes. Its total wave function, Ψ has to be antisymmetric in order to satisfy quantum-mechanical symmetry requirement. Under such condition, interchange of any 2 particles (A and B) of different states, ψ_i and ψ_j ($j \neq i$) will result in change of sign, hence the wave function for Fermions is in the form of

$$\Psi_{i,j}(C_A, C_B) = \psi_i(C_A)\psi_j(C_B) - \psi_i(C_B)\psi_j(C_A). \quad (12)$$

The negative sign in Eq. (12) that fulfils antisymmetric requirement is actually due to one of the eigenvalue of exchange operator [38], $\mathbf{P} = -1$. The other eigenvalue, $\mathbf{P} = +1$ is for Bosons. C_A and C_B denote all the necessary cartesian coordinates of the particles A and B respectively. Equation (12) is nothing but Pauli's exclusion principle. The one-particle energies E_1, E_2, \dots, E_m for the corresponding one-particle quantum states q_1, q_2, \dots, q_m can be rewritten as $(E_{is} \pm E_I)_1, (E_{is} \pm E_I)_2, \dots, (E_{is} \pm E_I)_m$. Note here that $E_{is} = E_{initial\ state}$. It is also important to realize that $E_{is} + E_I = E_{electrons}$ and $E_{is} - E_I = E_{holes}$. Subsequently, the latter $(E_{is} \pm E_I)_i$ version where $i = 1, 2, \dots, m$ with E_I as an additional inclusion will be used to derive iFDS and its Lagrange

multipliers. This $\pm E_I$ is inserted carefully to justify that an electron to occupy a higher state N from initial state M is more probable than from initial state L if condition $E_I(M) < E_I(L)$ at certain T is satisfied. As for a hole to occupy a lower state M from initial state N is more probable than to occupy state L if the same condition above is satisfied. E_{is} is the energy of a particle in a given system at a certain initial state and ranges from $+\infty$ to 0 for electrons and 0 to $-\infty$ for holes. In contrast, standard FDS only requires E_i ($i = 1, 2, \dots, m$) as the energy of a particle at a certain state.

Denoting n as the total number of particles with n_1 particles with energy $(E_{is} \pm E_I)_1$, n_2 particles with energy $(E_{is} \pm E_I)_2$ and so on implies that $n = n_1 + n_2 + \dots + n_m$. As a consequence, the number of ways for q_1 quantum states to be arranged among n_1 particles is given as

$$P(n_1, q_1) = \frac{q_1!}{n_1!(q_1 - n_1)!}. \quad (13)$$

Now it is easy to enumerate the total number of ways for q quantum states ($q = q_1 + q_2 + \dots + q_m$) to be arranged among n particles, which is

$$P(n, q) = \prod_{i=1}^{\infty} \frac{q_i!}{n_i!(q_i - n_i)!}. \quad (14)$$

The most probable configuration at certain T can be obtained by maximizing $P(n, q)$ subject to the restrictive conditions

$$\sum_i^{\infty} n_i = n, \sum_i^{\infty} dn_i = 0. \quad (15)$$

$$\sum_i^{\infty} (E_{is} \pm E_I)_i n_i = E, \sum_i^{\infty} (E_{is} \pm E_I)_i dn_i = 0. \quad (16)$$

The method of Lagrange multipliers [38] can be employed to maximize Eq. (14). Hence, a new function, $F(x_1, x_2, \dots, \mu, \lambda, \dots) = f + \mu f_1 + \lambda f_2 + \dots$ is introduced and all its derivatives are set to zero

$$\frac{\partial F}{\partial x_n} = 0; \quad \frac{\partial F}{\partial \mu} = 0; \quad \frac{\partial F}{\partial \lambda} = 0. \quad (17)$$

As such, one can let the new function in the form of

$$F = \ln P + \mu \sum_i^{\infty} dn_i + \lambda \sum_i^{\infty} (E_{is} \pm E_I)_i dn_i. \quad (18)$$

After applying Stirling's approximation, $\partial F / \partial n_i$ can be written as

$$\begin{aligned} \frac{\partial F}{\partial n_i} &= \ln(q_i - n_i) - \ln n_i + \mu + \lambda(E_{is} \pm E_I)_i \\ &= 0. \end{aligned} \quad (19)$$

Thus, the Fermi-Dirac statistics based on ionization energy is simply given by

$$\frac{n_i}{q_i} = \frac{1}{\exp[\mu + \lambda(E_{is} \pm E_I)_i] + 1}. \quad (20)$$

Importantly, the total energy, E in iFDS can be obtained from Eq. (16), which is

$$\begin{aligned} E &= \sum_i^{\infty} (E_{is} \pm E_I)_i n_i \\ &= \sum_i^{\infty} \frac{\hbar^2}{2m} [\mathbf{k}_{is}^2 \pm \mathbf{k}_I^2]_i n_i \\ &= \frac{\hbar^2}{2m} [\mathbf{k}_{is}^2 \pm \mathbf{k}_I^2] = \frac{\hbar^2}{2m} \mathbf{k}^2. \end{aligned} \quad (21)$$

$\mathbf{k}_I = \mathbf{k}_{ionized\ state}$, and the \pm sign is solely to indicate that the energy corresponds to electrons is $0 \rightarrow +\infty$ while $0 \rightarrow -\infty$ is for the holes, which satisfy the particle-hole symmetry. Consequently, Eq. (21) also implies that iFDS does not violate the degeneracy requirements. By utilizing Eq. (20) and taking $\exp[\mu + \lambda(E \pm E_I)] \gg 1$, one can arrive at the probability function for electrons in an explicit form as

$$f_e(\mathbf{k}_{is}) = \exp \left[-\mu - \lambda \left(\frac{\hbar^2 \mathbf{k}_{is}^2}{2m} + E_I \right) \right], \quad (22)$$

Similarly, the probability function for the holes is given by

$$f_h(\mathbf{k}_{is}) = \exp \left[\mu + \lambda \left(\frac{\hbar^2 \mathbf{k}_{is}^2}{2m} - E_I \right) \right]. \quad (23)$$

The parameters μ and λ are the Lagrange multipliers. $\hbar = h/2\pi$, h = Planck constant and m is the charge carriers' mass. Note that E has been substituted with $\hbar^2 \mathbf{k}^2 / 2m$. In the standard FDS, Eqs. (22) and (23) are simply given by, $f_e(\mathbf{k}) = \exp[-\mu - \lambda(\hbar^2 \mathbf{k}^2 / 2m)]$ and $f_h(\mathbf{k}) = \exp[\mu + \lambda(\hbar^2 \mathbf{k}^2 / 2m)]$. Equation (15) can be rewritten by employing the 3D density of states' (DOS) derivative, $dn = V \mathbf{k}_{is}^2 d\mathbf{k}_{is} / 2\pi^2$, Eqs. (22) and (23), that eventually give

$$n = \frac{V}{2\pi^2} e^{-\mu} \int_0^{\infty} \mathbf{k}^2 \exp \left[-\lambda \frac{\hbar^2 \mathbf{k}^2}{2m} \right] d\mathbf{k}$$

$$\begin{aligned}
&= \frac{V}{2\pi^2} e^{-\mu} \int_0^\infty \mathbf{k}_{is}^2 \exp \left[-\lambda \frac{\hbar^2 \mathbf{k}_{is}^2}{2m} - \lambda \frac{\hbar^2 \mathbf{k}_I^2}{2m} \right] d\mathbf{k}_{is} \\
&= \frac{V}{2\pi^2} e^{-\mu - \lambda E_I} \int_0^\infty \mathbf{k}_{is}^2 \exp \left[-\lambda \frac{\hbar^2 \mathbf{k}_{is}^2}{2m} \right] d\mathbf{k}_{is}, \quad (24)
\end{aligned}$$

$$p = \frac{V}{2\pi^2} e^{\mu - \lambda E_I} \int_{-\infty}^0 \mathbf{k}_{is}^2 \exp \left[\lambda \frac{\hbar^2 \mathbf{k}_{is}^2}{2m} \right] d\mathbf{k}_{is}. \quad (25)$$

The respective solutions for Eqs. (24) and (25) are

$$\mu + \lambda E_I = -\ln \left[\frac{n}{V} \left(\frac{2\pi\lambda\hbar^2}{m} \right)^{3/2} \right], \quad (26)$$

$$\mu - \lambda E_I = \ln \left[\frac{p}{V} \left(\frac{2\pi\lambda\hbar^2}{m} \right)^{3/2} \right]. \quad (27)$$

Note that Eqs. (26) and (27) simply imply that $\mu_e(iFDS) = \mu(T=0) + \lambda E_I$ and $\mu_h(iFDS) = \mu(T=0) - \lambda E_I$. In fact, $\mu(FDS)$ need to be varied accordingly with doping, on the other hand, iFDS captures the same variation due to doping with λE_I in which, $\mu(T=0)$ is fixed to be a constant (independent of T and doping). Furthermore, using Eq. (16), one can obtain

$$\begin{aligned}
E &= \frac{V\hbar^2}{4m\pi^2} e^{-\mu(FDS)} \int_0^\infty \mathbf{k}^4 \exp \left[-\lambda \frac{\hbar^2 \mathbf{k}^2}{2m} \right] d\mathbf{k} \\
&= \frac{V\hbar^2}{4m\pi^2} e^{-\mu(T=0)} \int_0^\infty \mathbf{k}_{is}^4 \exp \left[-\lambda \frac{\hbar^2 \mathbf{k}_{is}^2}{2m} - \lambda \frac{\hbar^2 \mathbf{k}_I^2}{2m} \right] d\mathbf{k}_{is} \\
&= \frac{V\hbar^2}{4m\pi^2} e^{-\mu(T=0) - \lambda E_I} \int_0^\infty \mathbf{k}_{is}^4 \exp \left[-\lambda \frac{\hbar^2 \mathbf{k}_{is}^2}{2m} \right] d\mathbf{k}_{is} \\
&= \frac{3V}{2\lambda} e^{-\mu(T=0) - \lambda E_I} \left[\frac{m}{2\pi\lambda\hbar^2} \right]^{3/2} \quad (28)
\end{aligned}$$

$$= \frac{3V}{2\lambda} e^{-\mu(FDS)} \left[\frac{m}{2\pi\lambda\hbar^2} \right]^{3/2}. \quad (29)$$

Again, Eq. (28) being equal to Eq. (29) enable one to surmise that the total energy considered in FDS and iFDS is exactly the same. Quantitative comparison between Eq. (28) and with the energy of a 3D ideal gas, $E = 3nk_B T/2$, after substituting Eq. (26) into Eq. (28) will enable one to determine λ . It is found that λ remains the same as $1/k_B T$. Basically, at constant temperature ($T > 0$), FDS predicts the distribution spectrum if E is varied, relying on external inputs such as band gap (E_g) and/or Fermi level ($E_F(T)$). On the other hand, iFDS

needs only E_I as an external input to predict the variation of E , without relying on E_g and/or $E_F(T)$ at all, and subsequently its distribution spectrum can be obtained as well. Notice that E_F comes into iFDS as $E_F^0 = \text{constant}$, independent of T and doping. E_F^0 denotes the Fermi level at 0 K. In fact, iFDS and FDS take different approach in term of energy levels and Fermions' excitations to arrive at the same distribution spectrum. In simple words, iFDS is new in a sense that it gives one an alternative route to obtain the Fermions' distribution spectrum in which, FDS needs $E_F(T)$ and/or E_g while iFDS needs only E_I to arrive at the same distribution spectrum. Hence, based on the accuracy of these input parameters, one can choose either FDS or iFDS to be used for one's theoretical models.

5. Conclusions

In conclusion, the transport properties of $\text{Ga}_{1-x}\text{Mn}_x\text{As}$, $\text{La}_{1-x}\text{Ca}_x\text{MnO}_3$ and $\text{Mn}_x\text{Ge}_{1-x}$ can be characterized with a model consists of ionization energy based Fermi-Dirac statistics coupled with spin disorder scattering mechanism. This model has been able to explain the evolution of resistivity's curves with respect to temperature and Mn doping. The arguments for the incompatibility between the calculated and experimentally determined normalized magnetization is based on the total current's tendency to obey the principle of least action. The validity of $E_I + E_F$ and $M_\rho(T, M_0)$ have been justified quantitatively by computing p and $M_\rho(T)/M_0$ respectively, which are in excellent agreement with the experimental results. However, the magnitudes of A and B are not diagnosed due to unknown reliable values of A_h , J_{ex} and E_F . To this end, the variation of hole mobilities and dielectric constant with doping, the influence of multiple exchange interaction and energy gap above T_C should be investigated experimentally.

Acknowledgments

The author is grateful and beholden to Arulsamy Inasimuthu, Sebastiammal Inasimuthu, Arokia Das Anthony and Cecily Arokiam of CMG-A for their extended financial aid. ADA also thanks Bryne J.-Y. Tan, Jasper L. S. Loverio and Hendry Izaac Elim for their kind help with figure preparations and references.

-
- [1] R. Horyn, A. Sikora, E. Bukowska, Physica C 387 (2003) 277.
 - [2] N. Chan, P. Q. Niem, H. N. Nhat, N. H. Luong, N. D. Tho, Physica B 327 (2003) 241.

FIG. 1: Equation (7) has been employed to fit the experimental $\rho(T)$ plots for $\text{Ga}_{1-x}\text{Mn}_x\text{As}$ as given in a) whereas Eq. (9) is used to fit the plots in b). All fittings are indicated with solid lines. b) is actually for annealed non-ferromagnetic $\text{Ga}_{0.930}\text{Mn}_{0.070}\text{As}$ samples. c) and d) show the T variation of calculated $M_\alpha(T)/M_{4.2}$ ($\alpha = K, \text{TD}, \rho$) with $S = 1$ for $x = 0.060$ and 0.070 respectively. $M_K(T)/M_{4.2}$ is also calculated with $S = 5/2$. The experimental $M_{exp}(T)/M_{4.2}$ plot for $x = 0.070$ (as grown) is shown in d).

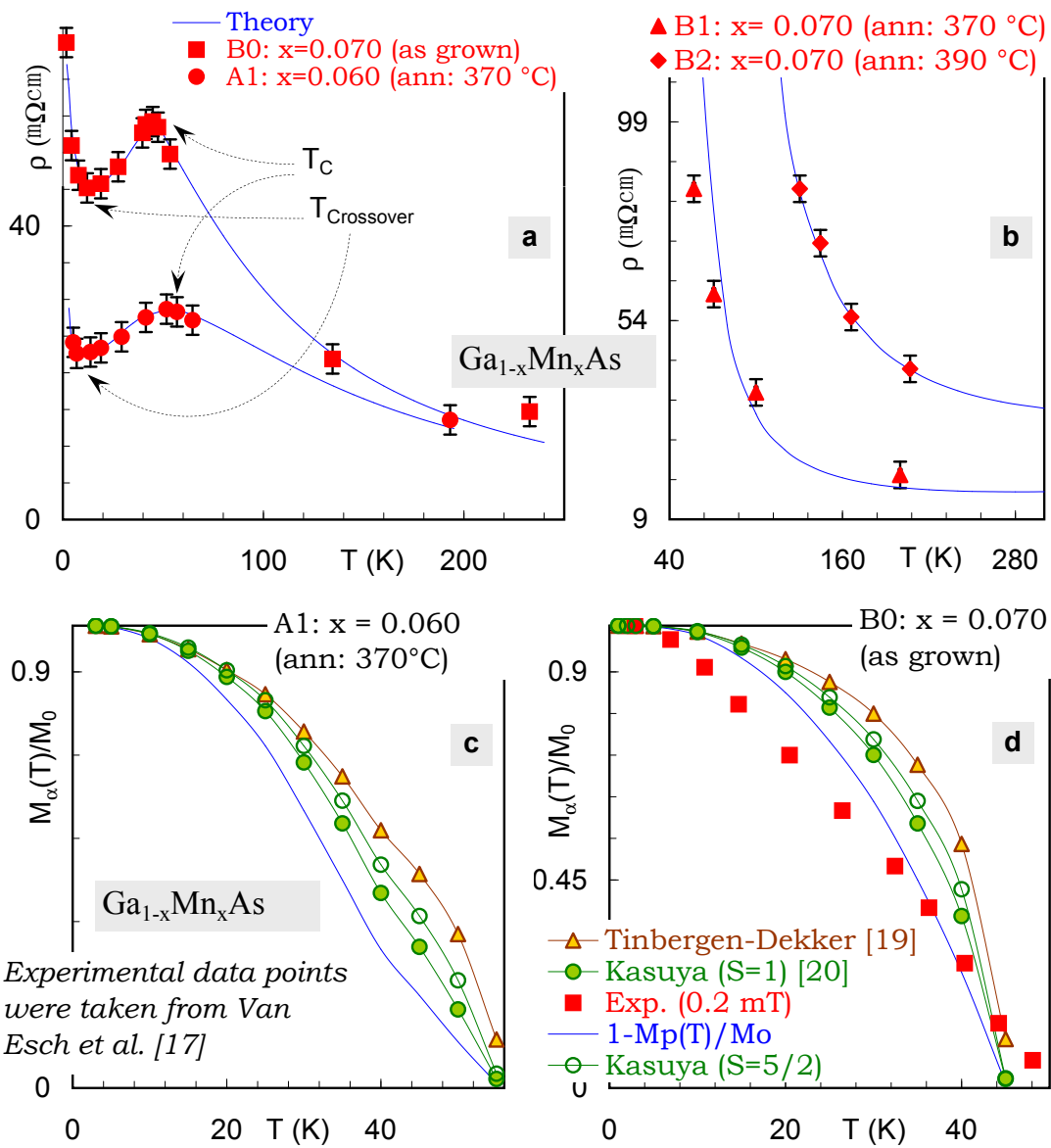
FIG. 2: Experimental plots of $\rho(T)$ for $\text{La}_{1-x}\text{Ca}_x\text{MnO}_3$ at $x = 0.1, 0.2$ and 0.2 (6 T) have been fitted with Eq. (6) as depicted in a) and b). All fittings are indicated with solid lines. Whereas c) and d) show the T variation of calculated $M_\alpha(T)/M_{4.2}$ ($\alpha = K, \rho$) with $S = 1$ for $x = 0.1$ and 0.2 respectively. The experimental $M_{exp}(T)/M_{4.2}$ plot for $x = 0.2$ is given in d).

- [3] S. Ju, H. Sun, Z.-Y. Li, Phys. Lett. A 300 (2002) 666.
- [4] A. D. Hernandez, C. Hart, R. Escudero, O. Ares, Physica B 320 (2002) 64.
- [5] D. -S. Yang, A. N. Ulyanov, M. -H. Phan, I. Kim, B. -K. Ahn, J. R. Rhee, J. S. Kim, C. Nguyen, S. -C. Yu, Physica B 327 (2003) 183.
- [6] A. Abramovich, R. Demin, R. Koroleva, A. Michurin, K. A. Maslov, Ya. M. Mukovskii, Phys. Lett. A 259 (1999) 57.
- [7] R. H. Heffner, J. E. Sonier, D. E. Maclaughlin, G. J. Nieuwenhuys, F. Mezei, G. Ehlers, J. F. Mitchell, S. W. Cheong, Physica B 326 (2003) 494.
- [8] V. G. Prokhorov, G. G. Kaminsky, V. A. Komashko, Y. P. Lee, I. I. Kravchenko, Physica B 334 (2003) 403.
- [9] J. R. Sun, C. F. Yeung, K. Zhao, H. K. Wong, C. M. Xiong, B. G. Shen, Physica B 334 (2003) 310.
- [10] C. L. Mei, Z. P. Xiong, H. -U. Habermeier, Physica B 327 (2003) 163.
- [11] A. I. Coldea, S. J. Blundell, C. A. Steer, F. L. Pratt, D. Prabhakaran, J. F. Mitchell, Physica B 326 (2003) 500.
- [12] R. Demin, Koroleva, R. Szymczak, H. Szymczak, Phys. Lett. A 296 (2002) 139.

FIG. 3: a) Equation (7) has been employed to fit the experimental $\rho(T)$ plots for $\text{Mn}_{0.02}\text{Ge}_{0.98}$. The plot with additional constraint, $dM_\rho(T)/dT = 0$ on Eq. (7) is also given to emphasize the influence of $M_\rho(T)/M_0$ for an accurate fitting. In these two plots, $A = 25$, $B = 1060$ and $E_I + E_F = 15$ K. The T -dependence of $\rho(T)$ in accordance with J_e only, ignoring J_{se} is calculated with Eq. (9), which lacks the ability to capture the experimental $\rho(T, x = 0.02)$. In this case, $A_h = 1.8$ and $E_I + E_F = 15$ K. Both $E_I + E_F = 15$ K and $E_I + E_F = 80$ K give p in the order of 10^{19} cm^{-3} using Eq. (6) and $m_h^* = \text{rest mass}$. b) Shows the T variation of $M_\alpha(T)/M_0$ ($\alpha = K, \rho, exp$) for $x = 0.02$. Notice the inequality, $M_K(T)/M_0 > M_\rho(T)/M_0 > M_{exp}(T)/M_0$ that arises as a result of the principle of least action. The T -dependence of $M_\alpha(T)/M_0$ is close to the $\text{Ga}_{1-x}\text{Mn}_x\text{As}$ DMS, rather than the traditional manganites. As such, this behavior is suspected to be associated with the multiple exchange interaction.

TABLE I: Calculated values of T independent electron-electron scattering rate constant (A), B , which is a function of T independent spin disorder scattering rate constant and spin exchange energy (J_{ex}) as well as the ionization energy (E_I). All these parameters are for Mn doped $\text{Ga}_{1-x}\text{Mn}_x\text{As}$ (as grown and annealed at 370 °C, 390 °C) and Ca doped $\text{La}_{1-x}\text{Ca}_x\text{MnO}_3$ (measured at 0 and 6 T) systems. All $\text{Ga}_{1-x}\text{Mn}_x\text{As}$ samples were measured at 0 T.

- [13] A. Solontsov, C. Lacroix, Phys. Lett. A 296 (2002) 199.
- [14] U. Yu, Y. Jo, B. I. Min, Physica B 328 (2003) 117.
- [15] D. A. Filippov, R. Z. Levitin, A. N. Vasilev, T. N. Voloshok, R. Suryanarayanan, Physica B 327 (2003) 155.
- [16] I. Medvedeva, A. Maignan, K. Barner, Yu. Bersenev, A. Roev, B. Raveau, Physica B 325 (2003) 57.
- [17] A. Van Esch, L. Van Bockstal, J. De Boeck, G. Verbanck, A. S. van Steenbergen, P. J. Wellmann, B. Grietens, R. Bogaerts, F. Herlach, G. Borghs, Phys. Rev. B 56 (1997) 13103.
- [18] R. Mahendiran, S. K. Tiwary, A. K. Raychaudhuri, T. V. Ramakrishnan, R. Mahesh, N. Rangavittal, C. N. R. Rao, Phys. Rev. B 53 (1996) 3348.
- [19] Tineke Van Peski-Tinbergen, A. J. Dekker, Physica 29 (1963) 917.
- [20] T. Kasuya, Prog. Theor. Phys. 16 (1956) 58.
- [21] H. Ohno, Science 281 (1998) 951.
- [22] Y. D. Park, A. T. Hanbicki, S. C. Erwin, C. S. Hellberg, J. M. Sullivan, J. E. Matson, T. F. Ambrose, A. Wilson, G. Spanos, B. T. Jonker, Science 295 (2002) 651.
- [23] A. Das Arulsamy, cond-mat/0212202 (Unpublished).
- [24] A. Das Arulsamy, Physica C 356 (2001) 62.
- [25] A. Das Arulsamy, Phys. Lett. A 300 (2002) 691.
- [26] A. Das Arulsamy, P. C. Ong, M. T. Ong, Physica B 325 (2003) 164.
- [27] A. Das Arulsamy, Physica B 352 (2004) 285.
- [28] A. Das Arulsamy, Physica C 420 (2005) 95.
- [29] A. Das Arulsamy, in: Paul S. Lewis (Ed.), Superconductivity Research at the Leading Edge, Nova Science Publishers, New York, 2004, pp. 45-57; A. Das Arulsamy, cond-mat/0408613.
- [30] A. Das Arulsamy, Phys. Lett. A 334 (2005) 413.
- [31] J. J. Tu, G. L. Carr, V. Perebeinos, C. C. Homes, M. Strongin, P. B. Allen, W. N. Kang, E. -M. Choi, H. -J. Kim, S. -I. Lee, Phys. Rev. Lett. 87 (2001) 277001.
- [32] N. Mannella, A. Rosenhahn, C. H. Booth, S. Marchesini, B. S. Mun, S. -H. Yang, K. Ibrahim, Y. Tomioka, and C. S. Fadley, Phys. Rev. Lett. 92 (2004) 166401.
- [33] A. Banerjee, B. K. Chaudhuri, A. Sarkar, D. Sanyal, D. Banerjee, Physica B 299 (2001) 130.
- [34] A. Banerjee, S. Pal, B. K. Chaudhuri, J. Chem. Phys. 115 (2001) 1550.
- [35] L. Van Bockstal, A. Van Esch, R. Bogaerts, F. Herlach, A. S. van Steenbergen, J. De Boeck, G. Borghs, Physica B 246-247 (1998) 258.
- [36] K. Ando, T. Hayashi, M. Tanaka, A. Twardowski, J. Appl. Phys. 53 (1998) 6548.
- [37] M. J. Winter (<http://www.webelements.com>).
- [38] D. J. Griffiths, Introduction to Quantum Mechanics, Prentice-Hall, New Jersey, 1995.



Sample	Ann. $T(H)$ °C(Tesla)	A [Calc.]	B [Calc.]	$E_I + E_F$ [Calc.] K(meV)	$T_C(T_{cr})$ K [17,18]
Ga _{0.940} Mn _{0.060} As [1]	370 (0)	4.5	400	8 (0.69)	50 (10)
Ga _{0.930} Mn _{0.070} As [1]	As grown (0)	9.2	400	12 (1.04)	45 (12)
Ga _{0.930} Mn _{0.070} As [1]	370 (0)	0.02	~	280 (24.2)	~
Ga _{0.930} Mn _{0.070} As [1]	390 (0)	0.03	~	400 (34.5)	~
La _{0.9} Ca _{0.1} MnO ₃ [2]	~ (0)	10	0.65	1400 (121)	222 (~)
La _{0.8} Ca _{0.2} MnO ₃ [2]	~ (0)	10	1.2	1300 (112)	246 (~)
La _{0.8} Ca _{0.2} MnO ₃ [2]	~ (6)	5	3.2	900 (78)	251 (~)

